RSC Advances

ROYAL SOCIETY OF CHEMISTRY

www.rsc.org/advances

High yield synthesis of nano-size g-C_3N_4 derivatives by dissolve-regrowth method with enhanced photocatalytic ability

Yuanguo Xu,[a] Meng Xie,[b] Shuquan Huang,[a] Hui Xu*,[a] Haiyan Ji,[c] Jiexiang Xia,[a] Yeping Li,[b] Huaming Li*[a]

[a]*School of Chemistry and Chemical Engineering, Jiangsu University, 301 Xuefu Road, Zhenjiang, 212013, P R China*

[b]*School of Pharmacy, Jiangsu University, 301 Xuefu Road, Zhenjiang, 212013, P R China*

[c]*School of Chemistry and Chemical Engineering, 301 Xuefu Road, Zhenjiang, 212013, P R China*

Keywords:

g-C_3N_4, HNO_3, photocatalyst, protonation, visible light

Abstract:

Nano-size g-C_3N_4 derivatives were fabricated by a simple dissolve-regrowth method in HNO_3 solution and followed by a calcination process. The X-ray diffraction (XRD), Z-potential, Elemental analyzer and IR are used to investigate the structure, composition and the properties of the samples. Scanning electron microscopy (SEM) show the average size of the nano-size g-C_3N_4 derivatives increase with the increasing calcination temperature. The methyl orange (MO) dye was used as the target pollutant to investigate the photoactivity of the samples. The pure g-C_3N_4 only can degrade about 1.1 % MO, while the g-C_3N_4 derivatives calcined at 300℃ can decompose about 31.9 % of MO in 4 h. Besides, when a small amount of methylene blue (MB) solution was introduced, the g-C_3N_4-HNO_3-300 can decompose about 75.8 % in 4 h. The photoactivity of g-C_3N_4 was greatly enhanced after the modification process (especially with the assistance of MB). Additional, this work supplied a simple method to modify materials with enhanced photoactivity. At last, the possible reactive species and the possible mechanism were proposed based on the Electron spin resonance (ESR) and XPS results.

Introduction

Graphitic carbon nitride (g-C_3N_4) as a novel metal-free material, possess a suitable band gap of 2.7 eV and can utilize the visible light. It has been widely investigated in the photodegradation of dyes in water, CO_2 activation, hydrogen production and many other reactions [1]. Meanwhile, g-C_3N_4 is stable and can be easily prepared by calcination of abundant and cheap materials, such as urea, dicyandiamide, melamine and so on. Therefore, it has attracted more attention and efforts to investigate its potential application.

Although the pure g-C_3N_4 possesses so many advantages, it still suffers the high electron-hole recombination, low surface area, low quantum efficiency and so on. In order to solve these problems to make the g-C_3N_4 more valuable, many strategies have been used to modify the g-C_3N_4, including (1) Combined with metal and metal oxides: it can enhance the electron-hole separation ability and enhance its photoactivity. Au/g-C_3N_4 can improve the H_2 generation and reduce 4-nitrophenol to 4-aminophenol performance than g-C_3N_4 [2]. ZnO/g-C_3N_4 with well-matched overlapping band-structure showed much higher photoactivity in degrading MB dye than the single g-C_3N_4 [3]. In addition, many other metal and metal oxides have been used to modify g-C_3N_4 and exhibit improved performance. Such as Fe [4], Pt [5], TiO_2[6], WO_3[7] and Bi_2O_3 [8]. (2) Combined with metal composition: Core/shell structure g-C_3N_4/$BiPO_4$ was fabricated and the thickness of the g-C_3N_4 shell can be controlled. The enhancing photocatalytic activity of the sample was benefit from the charge transfer ability of the g-C_3N_4 shell. The photoactivity of the composite can be determined by tuning the thickness of the g-C_3N_4 [9]. g-C_3N_4/$SmVO_4$ composite can also enhance the photocatalytic ability [10]. There are many other typical compound hybrid with g-C_3N_4, such as g-C_3N_4/TaON [11], g-C_3N_4/Bi_2WO_6 [12], BiOBr-g-C_3N_4 [13] and so on. All of these works can utilize the visible light more efficiently and enhance the photoactivity in degrading dye. (3) Non-metal elements dope and hybrids: Many non-metal elements were used to modify the g-C_3N_4 to extend its light response range, and hence promote their performance, including O [14], B [15], F [16], P [17], V [18] and so on. Oppositely, Liu et al. [19] reported that the doping S leads to the reduced absorbance of light, but the widening and upshifting of its VB enhanced the photoactivity of the S doped g-C_3N_4. There are also some other non-metal materials were used to hybrid with the g-C_3N_4 to enhanced its electron-hole pair separation ability, such as C [20], P [21] and graphene[22-25]. (4) Preparation

of mesoporous g-C_3N_4: Template method was used to control the morphological properties of g-C_3N_4, the surface area of g-C_3N_4 can be significantly enhanced [26-28], and the enhancing performance of the g-C_3N_4 was thus acquired. Using two raw materials calcined at the same time can get the mesoporous g-C_3N_4 and leads to its enlarged surface area, which is beneficial to its photoactivity [29]. (5) Fabrication of nanosheet g-C_3N_4: Because the graphene can be obtained by exfoliated the graphite and hence possess advantage in the charge transfer [30] and the structure of g-C_3N_4 is similar to the graphite, many methods have been tried to exfoliate bulk g-C_3N_4 into nanosheet g-C_3N_4. Ultrasonic process was used to treat the bulk g-C_3N_4 in different solutions, and the nanosheet g-C_3N_4 do obtained and showed better performance than that of bulk g-C_3N_4 [31, 32]. Thermal oxidation method can also exfoliate bulk g-C_3N_4 into nanosheet g-C_3N_4 and the as-prepared sample showed higher photoactivity than the bulk one [33]. H_2SO_4 can exfoliate bulk g-C_3N_4 into single atomic layer g-C_3N_4 and the single atomic layer g-C_3N_4 showed higher photocatalytic H_2 production, pollutant decomposition activities and photocurrent generation [34].

Based on the above analysis, it can be seen that increasing the surface area of g-C_3N_4 is benefit for enhancing its photoactivity. Generally, the surface area of the g-C_3N_4 can be enlarged by two simple strategies: (1) Exfoliate the bulk g-C_3N_4 into few-layer or single-layer g-C_3N_4. (2) Using template method to get porous structure g-C_3N_4 with regular shape or heating two raw materials at the same time to obtain porous structure g-C_3N_4 without regular shape. However, exfoliate the bulk g-C_3N_4 by ultrasonic or thermal oxidation will leads to the very low productivity and the process of the template method is relatively complicated. Therefore, investigating a simple method with high yields of regular shape and small dimension of g-C_3N_4 is still a challenge.

As we know, the g-C_3N_4 can be protonated by HCl, and the protonated g-C_3N_4 possess a better dispersion property in water and higher ionic conductivity than that of the original g-C_3N_4 [35]. Although the g-C_3N_4 protonated by HCl possess a lot advantages, its size is still large. So, it is thought that if the g-C_3N_4 protonated by an acid with oxidizing ability, the bulk g-C_3N_4 may be "cut" into small size due to the strong oxidizing ability. Moreover, it may appear some group on the surface of g-C_3N_4, which may benefit to enhance its photoactivity. HNO_3 is an ideal acid, it can protonate the g-C_3N_4 to improve the dispersion property and have potential ability to oxidize

g-C_3N_4 and "cut" it into small size. There are several works have been reported, the raw materials were treated by HNO_3 and then calcined into g-C_3N_4. With the assistance of ethylene glycol, the final products can keep nanotube or micro strings shape with high yields [36, 37]. There is also other work reported that the g-C_3N_4 was fabricated first, and then treated by HNO_3 [38]. The obtained nano-size g-C_3N_4 showed good fluorescence property. However, these works did not have use the strong oxidation ability of the HNO_3 more intuitionistic.

Herein, we report nano-size g-C_3N_4 derivatives prepared by HNO_3 treating. The g-C_3N_4 was "cut" by the HNO_3 thoroughly and formed a transparent solution when the mixture of g-C_3N_4 and HNO_3 was heated. The nano-size g-C_3N_4 derivatives appeared when the solution cooled to room temperature. Then, the sample was washed to neutral and calcined at different temperature. The samples were characterized and the photoactivity was investigated. The hot HNO_3 not only "cut" the g-C_3N_4 into nano-size g-C_3N_4 derivatives with higher BET surface area, but also introduce certain group on the surface of g-C_3N_4 at the same time. The introduced group on the surface of g-C_3N_4 in the "cutting" process is necessary in keeping the nano-size of g-C_3N_4 in the calcination process. Furthermore, the protonated g-C_3N_4 can disperse in the solution much better, which is facile for the contact between the photocatalyst and the pollutant. These two characteristic is beneficial for nano-size g-C_3N_4 derivatives to degrade the pollutant.

It is known that the g-C_3N_4 can degrade the methylene blue (MB) [39] and Rhodamine B (RhB) [40] under visible light irradiation, but we found that it is helpless in degrading the Methyl Orange (MO) under visible light irradiation (the data is shown in this work). The HNO_3 modification is benefit for enhancing its photoactivity in decomposing MO. Besides, the nano-size g-C_3N_4 derivatives can be activated by MB (a pollutant but not the costly oxidant H_2O_2) to degrade MO more efficient, the sample achieved the aim of treatment of wastes with processes of wastes against one another. Besides, the degradation of two dyes at the same time is more similar to actual application.

2. Experimental Section

2.1. Chemicals

All the chemicals used in this experiment were reagent grade and without further purification.

g-C_3N_4 was prepared by directly heating dicyandiamide as our previous work[41].

2.2. The synthesis of the nano-size g-C_3N_4

The prepared g-C_3N_4 was put into HNO_3 and stirred for about 24 h and got a white suspension, the white suspension was then heated and changed into a clear and transparent aqueous. Then, the hot transparent aqueous was cooled to room temperature and a white material reformed. The g-C_3N_4 in HNO_3 occur a dissolve-regrowth process. The reformed white precipitate was collected and washed by water to the neutral, and then the white product was dried at 60℃ and the obtained sample was marked as g-C_3N_4-HNO_3, then the g-C_3N_4-HNO_3 was calcined at 300℃ (marked as g-C_3N_4-HNO_3-300), 500℃(marked as g-C_3N_4-HNO_3-500) for 2 h, respectively.

2.3. Characterization

The crystal phase was analyzed by X-ray diffraction (XRD) analysis on the AdvantXP4200 (American) in the 2θ range of 10º-40º. Scanning electron microscopy (SEM) of the samples was observed by a FE-SEM (JEOL JSM-7001F). UV-vis absorption spectra of the liquid samples were taken on a UV-vis spectrophotometer (UV-2450, Shimadzu Corporation, Japan). The UV-vis absorption spectra of the solids samples (in the diffuse reflectance spectra mode) were measured in solid state, and $BaSO_4$ powder was used as the substrate. Infrared (IR) spectra (KBr pellets) were recorded on Nicolet Model Nexus 470 IR equipment. X-ray photoemission spectroscopy (XPS) was measured on a PHI5300 with a monochromatic Mg Kα source to explore the elements on the surface. Photoluminescence (PL) spectra of the catalyst were measured on the QuantaMaster & TimeMaster Spectrofluorometer, QuantaMaster^{TM} 40 (Photon Technology International, Inc.) with excitation wavelength of 315 nm. The photocurrents were measured with an electrochemical analyzer (CHI660B, CHI Shanghai, Inc.) The Z-potential of the samples were tested on the Malvern ZEN3600. The composition of the samples was analyzed by Elemental analyzer (Flash 1112A). Electron spin resonance (ESR) spectra were recorded using JES FA200 (JEOL) equipped with a xenon lamp (with 420 nm filter) as the light source. 5,5-dimethyl-1-pyrroline-N-oxide (DMPO) was used to trap the signals of radicals spin.

2.4. Photocatalytic experiments

The application of the g-C_3N_4 and the modified composite in degrading organic dye methyl

orange (MO) was investigated under visible-light irradiation at 30℃. In a typical procedure, a 0.0700 g amount of the photocatalyst was suspended in 70 mL MO solution (10 mg/L). Before the lamp (300 W Xe arc lamp, with a cut-off filter provides visible light with $\lambda \geq 400$ nm) was turned on to start irradiation, the solution was stirred for 0.5 h in the dark to get the adsorption/desorption equilibrium between the photocatalyst and the dye. The solution was sampled at 0.5 h intervals and was centrifuged, and the above liquid was then monitored by UV-vis spectroscopy at 463 nm.

Results and discussion

3.1 The Z-potential of the g-C_3N_4 and the nano-size g-C_3N_4 derivatives

In order to investigate the change of the g-C_3N_4 after it reacted with HNO_3 and the calcination process, the Z-potential of the samples were investigated and the result are displayed in Fig. 1. The g-C_3N_4 possessed -33.2 mV indicated that its surface is negative polarity in the solution. When g-C_3N_4 was treated by HNO_3, its surface Z-potential value changed from -33.2 mV into 40 mV. The significant changes indicated that the g-C_3N_4 was successfully modified by HNO_3 and formed a new material. The Z-potential value of the g-C_3N_4-HNO_3 decreased into 11.8 mV after it was heating at 300℃ for 2 h and further decreased into -13.7 mV after it was heating at 500℃ for 2 h. This result indicated that the Z-potential of the material can be tuned through heating operation. It also suggests that the nano-size g-C_3N_4 derivatives may be recovered by heating treatment.

3.2 SEM and BET

The SEM was used to investigate the morphologies of the samples. Fig. 2 A shows the g-C_3N_4 display in the form of bulk morphology, the size distribution is widely and mainly in several micrometers. While the g-C_3N_4 was treated by HNO_3, the morphology changed a lot and in the form of nanorods (as shown in Fig. 2 B). The width of the nanorods is smaller than 100 nm and the length of it is mainly in the range of 200-400 nm. Its size is much smaller than that of bulk g-C_3N_4. This may leads to the increase of surface area.

The mixture of the HNO_3 and g-C_3N_4 can form a clear and transparent aqueous when it was heated. Then, the decreasing temperature of the mixture leads to the regrowth of the modified g-C_3N_4. The g-C_3N_4 in the HNO_3 solution occur a dissolve-regrowth process, which play a key

role in the formation of nano-size g-C_3N_4-HNO_3. It also suggests the "cut" ability of the HNO_3 is very strong (the possible formation schematic diagram was shown in Fig. 2 E). Fig. 2 C exhibits the morphology of the nanorod g-C_3N_4-HNO_3 after calcined at 300℃ for 2 h. It is obvious that the nanorod turned into nano-particles, the particle size is mainly in the range of 50-300 nm. The average size is much larger than the nanorod g-C_3N_4-HNO_3. When the heating temperature raised to 500℃, the sample occur a further condensation polymerization, which leads to its size become larger and much like the untreated g-C_3N_4. The raising heating temperature may leads to the decreasing photoactivity. The BET surface area of the samples are tested by N_2 adsorption, and the corresponding value of the g-C_3N_4, g-C_3N_4-HNO_3 and g-C_3N_4-HNO_3-300 are 5.85 m^2/g, 37.90 m^2/g and 16.06 m^2/g, respectively. The results show that the BET surface area of g-C_3N_4-HNO_3 is about 6.5 times as high as that of g-C_3N_4, this is in good accordance with the SEM result. Compared with the g-C_3N_4-HNO_3, the BET surface area of g-C_3N_4-HNO_3-300 obviously decreased after calcined at 300℃. It is probably due to the average size of g-C_3N_4-HNO_3-300 is much larger than that of g-C_3N_4-HNO_3 (as shown in Fig. 2B and C). Nevertheless, it is still 2.7 times as high as that of the g-C_3N_4. Its large BET surface area may be benefit to its photoactivity.

3.3 Element analysis and XRD

Element analysis and XRD were utilized to ascertain the structure and the constituents of the samples. The element composition results are shown in Table 1. The trace amount of H and O in the g-C_3N_4 may ascribe to its NH_2/NH group and the adsorbed CO_2, O_2 and H_2O [41]. The C/N atomic ratio of bulk g-C_3N_4 is 0.664. When the g-C_3N_4 was treated by HNO_3, the C/N atomic ratio reduced to 0.598 and H and O content increased obviously. The result clearly states that the content of H, N and O in the samples increased in certain form after g-C_3N_4 was treated by HNO_3. When the g-C_3N_4-HNO_3 was calcined at 300℃, the C/N atomic ratio increased to 0.624 (still much lower than that of the g-C_3N_4), and the H and O content decreased at the same time (still much higher than that of g-C_3N_4). This result indicated that the H, N and O in the sample decreased at the same time. When the treating temperature raised to 500℃, the C/N atomic ratio increased to 0.660 (much closer to the g-C_3N_4). It indicates that the modified g-C_3N_4 derivatives can be recovered by simple heating treatment. The constituent of the samples changed obviously with the thermal treatment, the above SEM result is in good accordance with the element analysis

results. When the calcination temperature up to 500℃ (close to the g-C_3N_4 formation temperature 540℃), the bulk particles reformed and the shape become similar to the g-C_3N_4. The small content difference between the g-C_3N_4-HNO_3-500 and the bulk g-C_3N_4 may be come from the little residual group on the surface which contains H, N and O. This may ascribed to the thermal temperature is not high enough to recover completely and it also indicates that the modification is relatively stable.

Fig.3 displays the XRD patterns of the as prepared g-C_3N_4, g-C_3N_4-HNO_3, g-C_3N_4-HNO_3-300 and g-C_3N_4-HNO_3-500. Fig. 3 a displays the XRD pattern of the g-C_3N_4, which possess two peaks at 27.4° and 12.9°. The two peaks ascribed to the typical (002) and (100) diffraction planes of g-C_3N_4. When the g-C_3N_4 was treated by HNO_3, the peak at 27.4° shift to 27.8° and a new peak at 12.3° appeared. The peak at 27.4° is a characteristic stacking peak of pi-conjugated g-C_3N_4 layers, which shifts from 27.4° shift to 27.8° (similar phenomenon has been reported [38]). It means a decrease in the interplanar stacking distance [14]. It also indicates the g-C_3N_4 was successfully protonated. Furthermore, the appearance of the new peak at 12.3° suggests that the g-C_3N_4 was not only protonated by HNO_3 (our previous work [39] shows that the protonation of g-C_3N_4 leads to the disappearance of the peak at around 12.9° but not occur a new peak.), but also occur other changes in the HNO_3 treating process. Consider the above results of the element analysis, it can be inferred that the new peak is mainly due to the modification of a group which contains N and O elements. The small peak appeared at 31° after the HNO_3 process may be due to the reaction between the g-C_3N_4 and the solution in the heating process [42].

Fig. 3 c shows the XRD of the g-C_3N_4-HNO_3 after calcined at 300℃. It is clear that the diffraction peak at 27.8° shift back to its original position and the peak at 12.3° does not shift, which may be ascribed to the part de-protonation of the g-C_3N_4-HNO_3 sample. The intensity of the peak at 12.3° enhanced means that the g-C_3N_4-HNO_3 sample with higher crystallinity [42]. Fig. 3 d shows the XRD of the g-C_3N_4-HNO_3 calcined at 500℃. It is obvious that the peak at 12.3° disappear, which further confirms that the heating treating treatment tends to recover the g-C_3N_4. It indicates that the mainly skeleton frame of the g-C_3N_4 was not destroyed.

3.4 IR

Fig. 4 exhibits the IR spectra of the samples. As shown in Fig. 4 a and b, the peak at 808 cm^{-1} is

ascribed to the s-triazine ring system of the g-C_3N_4 [43]. When the g-C_3N_4 was treated by HNO_3, this peak shows a little shift to lower wavenumber, which indicated the HNO_3 modification leads to the change of the chemical condition of the s-triazine ring system of the g-C_3N_4. The shift might be ascribed to the electrostatic interaction between the substitutional group and the adjacent C-N group. It also indicates that the structure of g-C_3N_4 still exist after the modification of the HNO_3. The appearance of the peak at 1087 cm^{-1} indicated the successfully protonation of g-C_3N_4, which has been confirmed in our previous work [39]. The peak at 885 cm^{-1} becomes unobvious and the appearance of a new peak at 608 cm^{-1} after the g-C_3N_4 treated by HNO_3, which are obviously different to the g-C_3N_4-HCl. This suggests that the g-C_3N_4-HNO_3 is not only the protonation of g-C_3N_4, but also changed into a new derivative [35]. Zou et al. [44] has reported that the g-C_3N_4 soaking samples showed a similar new peak at 615 cm^{-1}, they speculate the peak ascribed to SO_4^{2-}. In our case, the peak at 608 cm^{-1} may be a group comes from the HNO_3 or its reduced species. Besides, the peak still exist after the sample was calcined at 300℃ (as shown in Fig. 4 c), it indicates that the group is relatively stable. The 6 peaks centered at the region of 1200-1650 cm^{-1} are the typical peaks of g-C_3N_4 (as shown in Fig. 4a), which changed into 4 peaks and the position of the peaks has been changed (the g-C_3N_4 treated by HCl only occurred shift [39]). Chen et al. [14] reported the O-doped g-C_3N_4 appears changes in the IR spectra, some of the peak shift but the amount of the peak does not changed. This indicated that the g-C_3N_4-HNO_3 is also different to the O-doped g-C_3N_4. A band at 1311 cm^{-1} ascribed to the NO adsorption to hyponitrites (NO^-, $N_2O_2^{2-}$) [45]. All these suggested that g-C_3N_4-HNO_3 sample is a different derivative compared to g-C_3N_4-HCl or O-doped g-C_3N_4. Fig. 4 c is the IR of the g-C_3N_4-HNO_3 calcined at 300℃, it shows that all the peaks appeared at the similar positions to the g-C_3N_4-HNO_3, without obvious change in IR result. It suggests that the groups in the sample doesnot change obviously and the derivative g-C_3N_4-HNO_3 is a relative stable materials. The change of the sample has been observed in the XRD result. Fig. 4 d shows the g-C_3N_4-HNO_3 calcined at 500℃, it is clear that all of the peaks almost the same to the original g-C_3N_4. It suggests that the g-C_3N_4-HNO_3 sample can be recovered by calcination. This characteristic is very useful in the future experiment in preparation of nano-size original g-C_3N_4.

3.5 TG

Thermal property of g-C_3N_4 and g-C_3N_4-HNO_3 were investigated by TG and DTA in the temperature range from room temperature to 800℃ and the results are shown in Fig. 5. Fig. 5A shows the TG and DTA of the g-C_3N_4. The TG curve only occurs a small weight reduction when the temperature raise up to 550℃ (which may be ascribed to the adsorbed H_2O and air). It can be seen that an endothermic peak occurs at around 613℃, this may be attributed to the decomposition and vaporization of the g-C_3N_4 fragments [46].The endothermic peak occurs at about 743℃ is ascribed to the decomposition of the g-C_3N_4. When the temperature reached 750℃, the mass of the g-C_3N_4 reduced to zero. It means that the g-C_3N_4 completely decomposed at O_2 atmosphere before 750℃. Fig. 5 B shows the TG and DTA curve of g-C_3N_4-HNO_3. It is clear that the mass loss about 10 % when the temperature raised to about 100℃. The reduction of the mass may ascribed to the adsorbed air or H_2O. In the temperature between 100-200℃, the mass of the g-C_3N_4-HNO_3 reduced less than 5%. It indicates that the low temperature calcination does not change the g-C_3N_4-HNO_3 too much. After raising the calcination temperature, the mass of g-C_3N_4-HNO_3 gradually reduced without any obviously endothermic and exothermic peak until the temperature is higher than 550℃. The DTA curve suggests that the g-C_3N_4-HNO_3 did not occur significant endothermic or exothermic reaction between 200℃ and 550℃. This indicated that the modification of the g-C_3N_4-HNO_3 changed into original g-C_3N_4 in a relatively mild process (The proton and the modified group smoothly dissociate at the same time). Combined with the IR results, it can infer that the group modified on the g-C_3N_4 is relative stable. When the temperature was further raised to around 640℃, the g-C_3N_4-HNO_3 decomposed completely. The TG results suggested that the higher calcination temperature will leads to the low yield of the samples in the O_2 atmosphere.

3.6 The optical properties

The optical properties of the samples were investigated by DRS and PL, the corresponding results are shown in Fig. 6 and Fig. 7. From Fig.6 A, it can be seen that the absorption edge of g-C_3N_4 is about 420 nm, while the absorption edge of g-C_3N_4-HNO_3 shifts to about 360 nm. The shift of the absorption edge is consistent with the change of the color (from yellow to white). When the g-C_3N_4-HNO_3 was calcined at 300℃, the absorption edge shift to higher wavelength. It means that the g-C_3N_4-HNO_3-300 sample can utilize more visible light and may be possess higher

photoactivity. When the g-C_3N_4-HNO_3 was calcined at 500℃, the sample shows the similar absorption edge to that of the original g-C_3N_4 but with higher visible light absorption ability. Fig. 6 B shows the corresponding band gap of the g-C_3N_4, g-C_3N_4-HNO_3, g-C_3N_4-HNO_3-300 and g-C_3N_4-HNO_3-500 are 2.78 eV, 3.31 eV, 3.16 eV and 2.92 eV respectively. The band gap of the g-C_3N_4-HNO_3 is too large, which may result in deactivation.

PL spectra of the samples are shown in Fig. 7. It shows the emission peaks of the g-C_3N_4, g-C_3N_4-HNO_3, g-C_3N_4-HNO_3-300 and g-C_3N_4-HNO_3-500 are located at around 460 nm, 400 nm 410 nm and 459 nm, respectively. The emission peak of g-C_3N_4-HNO_3 shows a blue shift by about 60 nm, which is in consistent with its larger band gap than that of the g-C_3N_4. When the g-C_3N_4 was calcined at 300℃, the emission peak of the g-C_3N_4-HNO_3 shifts from 400 nm to 410 nm, which obviously shows the change of the g-C_3N_4-HNO_3 after it was calcined at 300℃. Combined the XRD results (the peak of g-C_3N_4-HNO_3 shift back after it was calcined at 300℃) and the PL results, it can infer that significant changes of the sample occurred in other properties. The emission peak of g-C_3N_4-HNO_3-500 shows the similar position to the pure g-C_3N_4. All of these are consistent with the DRS results.

3.7 XPS

The chemical state of the samples' surface was investigated by XPS (as shown in Fig. 8). The full scan spectra of the samples are shown in Fig. 8 A, it is clear that all of the samples contain the C, N and O. As shown in Fig. 8 A, the intensity of O 1 s in the g-C_3N_4-HNO_3 and g-C_3N_4-HNO_3-300 is much higher than that of pure g-C_3N_4, which may due to the reason that O in pure g-C_3N_4 is mainly come from the adsorbed air and H_2O, while the g-C_3N_4-HNO_3 and g-C_3N_4-HNO_3-300 sample contain O in the composite. Fig. 8 B shows the C 1s of the three samples, the g-C_3N_4 possess two peaks at 284.8 eV and 288.2 eV, the peak located at 284.8 eV is related to the carbon contamination [33] and the peak at 288.2 eV ascribed to the N=C–N_2 coordination [47]. It is obviously that all of the three samples have the peak at 284.8 eV, while the peak ascribed to the N=C–N_2 for the g-C_3N_4-HNO_3 sample appears a little shift, which means that the modification of the HNO_3 has changed the chemical condition of the C in the g-C_3N_4. Furthermore, when the g-C_3N_4-HNO_3 was calcined at 300℃, the peak shift back to its original position. It indicates that in the calcination process, certain reaction has happened and the

chemical condition of the C changed back. This result is in good accordance with the XRD result. It suggests that certain unstable group or element linked to the C in g-C_3N_4 after HNO_3 processing. Besides, it dissociated after calcination at 300℃. The change in the chemical condition may result in the change of the samples' photoactivity. Fig. 8 C shows the N 1s of the samples, which was deconvoluted into three peaks. The peak at 398.7 eV in the g-C_3N_4 is ascribed to sp^2-hybridized nitrogen (C=N–C) and the peaks at 400.0 eV and 401.2 eV assigned to the tertiary nitrogen (N–(C)3) groups[7]. As can be seen in Fig. 8 C, these peaks in g-C_3N_4 appears shift after it was modified by HNO_3, and they occur further shift after the modified sample was calcined at 300℃. These changes indicate that the chemical condition of N in the g-C_3N_4 changed after it was modified by HNO_3, and it occurred a further change after calcination. Fig. 8 D shows the O 1s of the samples, the peak at 532.4 eV in the g-C_3N_4 is ascribed to the adsorbed O species on the surface of the g-C_3N_4[7]. Besides, the other peak at 531.6 eV and 531.1 eV for the g-C_3N_4-HNO_3 and g-C_3N_4-HNO_3-300 is attributed to certain group contains O in the sample. This peak in the g-C_3N_4-HNO_3 sample shift after it was calcined, which means the chemical condition of O also changed. Based on the above results, it can infer the chemical condition of N and O changed at the same time. Combined with the Element analysis result, it suggests that the modification of HNO_3 leads to certain group (which containing O and N) has interaction with the N element in the g-C_3N_4 sample. The interaction can be further strengthened by heating. To further studied the influence of HNO_3 modification on the relative positions of CB and VB, VB XPS were obtained and showed in Fig. 8E. It is clear that the VB position of the g-C_3N_4 and g-C_3N_4-HNO_3-300 exhibit almost the same CB position. Combined with the UV-Vis results (the band gap of the g-C_3N_4 and g-C_3N_4-HNO_3-300 are 2.78 eV and 3.16 eV.), it can be inferred that the CB position of g-C_3N_4-HNO_3-300 is much lower than that of g-C_3N_4.

3.8 Enhanced photoactivity of the nano-size g-C_3N_4 derivatives

Fig. 9 shows the photocatalytic activity of g-C_3N_4 and nano-size g-C_3N_4 derivatives calcined at different temperature. MO was used as the target pollutant to evaluate their photo-degradation ability (In Fig. S1, it is clear that the MO did not decompose under visible light within 4 h without photocatalyst). The original g-C_3N_4 showed very low photocatalytic ability in degradation MO, only about 1.3 % MO was decomposed after 4 h (Fig. 9 a). The modified g-C_3N_4-HNO_3 showed

good adsorptivity but almost no photocatalytic activity (Fig. S2), which may because of its 3.31 eV band gap is too large to utilize the visible light energy. While the modified g-C_3N_4-HNO_3 calcined at 300℃ can decomposed about 31.9 % after 4 h (Fig. 1 e) under visible light irradiation (The degradation ability of g-C_3N_4-HNO_3 is not good compared to g-C_3N_4-HNO_3-300. Thus, it is believed that the structure and the proper band gap of the catalyst has the mainly effect on the degradation of MO rather than the trace amounts of residual acids on the surface of the nano-size g-C_3N_4 derivatives.) However, when the calcination temperature increased to 500℃, the degradation efficiency decreased to 17.8 % (Fig. 1 d). It may be because of the high calcination temperature leads to the recovery of the g-C_3N_4 structure and the aggregation of the samples (as shown in the SEM result).

Consider that some dye has the ability in sensitizing some catalyst and enhancing its photoactivity [48], MB was used in this experiment system. Several control experiments were done and the results are shown in Fig. 9, it is clear that the MO dye cannot be efficiently decomposed by the addition of 0.5 mL MB dye (only decomposed about 13.2 %) or g-C_3N_4/MB system (only decomposed about 8.8 %). When the g-C_3N_4-HNO_3-300/MB system was used, 75.8 % of MO was decomposed in 4 h. The corresponding absorption spectral change is shown in Fig. 10 (The introduced MB (10 mg/L) volume is only 0.5 mL, so the concentration of MB was diluted into 0.07 mg/L after it was poured into the 70 mL pollutant solution. Besides, some of the MB may be adsorbed on the surface of the catalyst. Therefore, the concentration of MB in the solution is too low to show obviously peak in the absorption spectral), it can be seen that the MO was indeed decomposed gradually. In Fig. 9, it is obvious that the addition of MB can efficiently enhance the photoactivity of the g-C_3N_4-HNO_3-300, while the g-C_3N_4 was not enhanced. As we know, g-C_3N_4 can degrade the MB under visible light irradiation [39]. So, it suggests that the MB molecular or its degraded products cannot efficient decompose the MO in the presence of the g-C_3N_4.

The reusability of the photocatalyst is a very important factor for the application. To investigate the stability of the g-C_3N_4-HNO_3-300, four successive photocatalytic experiments cycle runs were done. The result is shown in Fig. 11, it can be seen that no apparent decrease in photoactivity was observed. Based on the above experiment results, the g-C_3N_4-HNO_3-300 can be regarded as a stable photocatalyst.

The g-C_3N_4 can degrade the MB and RhB has been verified [39, 40], but it is helpless to do anything in degrading the MO dye. Why? Because the g-C_3N_4 almost cannot degrade the MO dye, it indicates that the photo-generated hole in the g-C_3N_4 cannot oxidize MO dye directly or indirectly and the related high reactive species (such as $O_2•^-$ [42]) derived from the photo-generated electron is also helpless to degrade the MO dye (Maybe the concentration of the $O_2•^-$ is very low in the solution). The g-C_3N_4-HNO_3 almost has no photoactivity in degradation of MO while the g-C_3N_4-HNO_3-300 has, which may because of its relative small band gap and the enhanced visible light absorption ability in the 400 nm - 800 nm. Considering the element analysis result (the content of H reduced after the calcination processing), it indicates that the enhanced photoactivity of the g-C_3N_4-HNO_3-300 is not mainly attributed to the residual H^+ that was not clean up on the surface of the sample.

In order to elucidate the reaction mechanism, ESR was used to detect the reactive species generated by the g-C_3N_4-HNO_3-300 (as shown in Fig. 12). Fig. 12 A shows that the characteristic peaks of $O_2•^-$ was not observed in g-C_3N_4-HNO_3-300 system with different conditions. This indicates that the $O_2•^-$ is not the main reactive species leads to its enhanced photoactivity. Fig. 12 B shows that the g-C_3N_4-HNO_3-300 cannot generate •OH without light irradiation, but it can generate weak characteristic peaks (with the intensity ratio 1 : 2 : 2 : 1) of DMPO-•OH under visible light irradiation. When the MB dye was introduced in the system, it also cannot generate characteristic peaks of DMPO-•OH in dark. However, the strong signal (with the intensity ratio 1 : 2 : 2 : 1) of DMPO-•OH appeared when the system was irradiated by visible light (in this condition, the MO can be efficiently degraded).

Based on the above analysis, it can be inferred that the MO dye can be efficiently degraded after the MB was introduced in the system, which is mainly because of the synergetic effect between the g-C_3N_4-HNO_3-300 and MB leads to the efficient generation of •OH. The g-C_3N_4-HNO_3-300 has the proper band gap and surface property to be activated by MB and generate enough •OH concentration. The generated •OH is the main active group in MO degradation. Wang et al. [49] has reported the similar results, the signals of spin-trapped DMPO−OH• were clearly observed while the superoxide radicals ($•O_2^-$) were relative low in g-C_3N_4 system. A possible mechanism was proposed based on Wang's work [4] and showed in Fig. 13. As shown in Fig. 13 A, under visible light irradiation, the g-C_3N_4-HNO_3 cannot be excited. It may be ascribed to two reasons: (1)

Its band gap is too larger to utilize the visible light. (2) There are some group or element connect to C (it has been explained in the XRD and XPS parts) in g-C_3N_4-HNO_3, C 2p orbital may be occupied by their electrons. The electrons occupied the C 2p orbital and repel the electron come from the N 2p orbital. However, the g-C_3N_4-HNO_3-300 can be excited by the visible light (as shown in Fig. 13 B). It may be ascribed to two reasons: (1) Its relative small band gap. (2) The group or element connected to C dissociated after the calcination at 300℃. The introduced group in the HNO_3 modification process is essential in tuning the C 2p position. The proper position and relative empty of the C 2p orbital is tend to receive the electrons come from the N 2p and the excited MB* [48, 50]. Because the position of N 2p is almost the same to that of pure g-C_3N_4 and the pure g-C_3N_4 almost has no ability in decomposing MO, the •OH should mainly come from the C 2p. As shown in Fig. 13 B, the electron in C 2p can generate •OH after a serial reactions. The introduced MB injects electrons into the C 2p and thus enhances the generation of •OH amount [51]. Therefore, the photoactivity of the g-C_3N_4-HNO_3-300 was significantly enhanced with the assistant of MB.

4. Conclusions

Nano-size g-C_3N_4-HNO_3-300 has been prepared through a facile HNO_3 modification and calcination without using temple or ultrasonic processing. The g-C_3N_4-HNO_3-300 has three advantages: (1) The protonation process made the g-C_3N_4-HNO_3-300 disperse better in the pollutant solution. It can utilize the large surface area efficiently to react with the pollutant. (2) The addition group in the g-C_3N_4-HNO_3-300 can keep the photocatalyst in small size after calcination. Besides, the addition group is essential in tuning the C 2p position. (3) The synthesized g-C_3N_4-HNO_3-300 can efficiently degrade the MO dye with the assistants of MB under visible light irradiation. This photocatalytic system avoids the using of any metal material or the expensive H_2O_2 as the oxidizing agent. The addition of MB (is also a pollutant) can act the role of H_2O_2 and achieve the aim of treatment of wastes with processes of wastes against one another with the presence of g-C_3N_4-HNO_3-300. The mixture of dyes has more similarity to a real wastewater. The catalyst is stable, efficient and reusable for the environmental applications.

Acknowledgements

This work is financially supported by the Jiangsu University Scientific Research Funding (No. 14JDG052), National Natural Science Foundation of China for Youths (No. 21407065, No. 21406094), China Postdoctoral Science Foundation (No.: 2014M551520, 2014M560399), Natural Science Foundation of Jiangsu Province for Youths (BK20140533).

Notes and references

[1] J. J. Zhu, P. Xiao, H. L. Li and S. A. C. Carabineiro, *ACS Appl. Mater. Interfaces,* 2014, **6,** 16449-16465.

[2] X. H. Li, X. C. Wang and M. Antonietti, *Chem. Sci.*, 2012, **3,** 2170-2174.

[3] D. M. Chen, K. W. Wang, T. Z. Ren, H. Ding and Y. F. Zhu, *Dalton Trans.*, 2014, **43,** 13105-13114.

[4] X. F. Chen, J. S. Zhang, X. Z. Fu, M. Antonietti and X. C. Wang, *J. Am. Chem. Soc.* 2009, **131,** 11658-11659.

[5] J. G. Yu, K. Wang, W. Xiao and B. Cheng, *Phys. Chem. Chem. Phys.,* 2014, **16,** 11492-11501.

[6] J. G. Yu, S. H. Wang, J. X. Low and W. Xiao, *Phys. Chem. Chem. Phys.,* 2013, **15,** 16883-16890.

[7] L. Y. Huang, H. Xu, Y. P. Li, H. M. Li, X. N. Cheng, J. X. Xia, Y. G. Xu and G. B. Cai, *Dalton Trans.,* 2013, **42,** 8606-8616.

[8] J. F. Zhang, Y. F. Hu, X. L. Jiang, S. F. Chen, S. G. Meng, X. L. Fu, *J. Hazard. Mater.*, 2014, **280**, 713-722

[9] J. Xu, Y. J. Wang, D. Li and Y. F. Zhu, *Adv. Funct. Mater.*, 2012, **22,** 1518-1524.

[10] T. T. Li, L. H. Zhao, Y. M. He, J. Cai, M. F. Luo and J. J. Lin, *Appl. Catal. B.,* 2013, **129,** 255-263.

[11] S. C. Yan, S. B. Lv, Z. S. Li and Z. G. Zou, *Dalton Trans.* 2010, **39,** 1488-1491.

[12] L. Ge, C. Han and J. Liu, *Appl. Catal. B.,* 2011, **108–109**, 100-107.

[13] L. Q. Ye, J. Y. Liu, Z. Jiang, T. Y. Peng and L. Zan, *Appl. Catal. B.,* 2013, 142-143, 1-7.

[14] J. H. Li, B. Shen, Z. H. Hong, B. Z. Lin, B. F. Gao and Y. L. Chen, *Chem. Commun.,* 2012, **48,** 12017-12019.

[15] S. C. Yan, Z. S. Li, Z. G. Zou, *Langmuir,* 2010, **26**, 3894-3901.

[16] Y. Wang, Y. Di, M. Antonietti, H. Li, X. Chen, X. Wang, *Chem. Mater.* 2010, **22,** 5119-5121.

[17] Y. Zhang, T. Mori, J. Ye and M. Antonietti, *J. Am. Chem. Soc.* 2010, **132,** 6294-6295.

[18] G. D. Ding, W. T. Wang, T. Jiang, B. X. Han, H. L. Fan and G. Y. Yang, *ChemCatChem,* 2013, **5,** 192-200.

[19] G. Liu, P. Niu, C. H. Sun, S. C. Smith, Z. G. Chen, G. Q. Lu and H. M. Cheng, *J. Am. Chem. Soc.* 2010, **132,** 11642-11648.

[20] Y. Zheng, Y. Jiao, J. Chen, J. Liu, J. Liang, A. J. Du, W. M. Zhang, Z. H. Zhu, S. C. Smith, M. Jaroniec, G. Q. Lu and S. Z. Qiao, *J. Am. Chem. Soc.,* 2011, **133,** 20116-20119.

[21] Y. P. Yuan, S. W. Cao, Y. S. Liao, L. S. Yin, C. Xue, *Appl. Catal. B.,* 2013 **140-141,** 164-168.

[22] Y. J. Zhang, T. Mori, L. Niu and J. H. Ye, *Energy Environ. Sci.,* 2011, **4,** 4517-4521.

[23] J. Q. Tian, Q. Liu, A. M. Asiri, K. A. Alamry and X. P. Sun, *ChemSusChem,* 2014, **7,** 2125-2130.

[24] G. Z. Liao, S. Chen, X. Quan, H. T. Yu and H. M. Zhao, *J. Mater. Chem.* 2012, **22**, 2721-2726.

[25] Q. J. Xiang, J. G. Yu and M Jaroniec, *J. Phys. Chem. C,* 2011, **115**, 7355-7363.

[26] J. Xu, H. T. Wu, X. Wang, B. Xue, Y. X. Li and Y. Cao. *Phys. Chem. Chem. Phys.,* 2013, **15,** 4510-4517.

[27] Y. S. Jun, E. Z. Lee, X. C. Wang, W. H. Hong, G. D. Stucky, A. Thomas, *Adv. Funct. Mater.* 2013, **23**, 3661-3667.

[28] Y. Fukasawa, K. Takanabe, A. Shimojima, M. Antonietti, K. Domen and T. Okubo, *Chem. Asian J.* 2011, **6,** 103-109.

[29] M. Zhang, J. Xu, R. L. Zong and Y. F. Zhu. *Appl. Catal. B.,* 2014, **147.** 229-235.

[30] Q. J. Xiang, J. G. Yu and M. Jaroniec, *Chem. Soc. Rev.,* 2012, **41,** 782-796.

[31] Enhanced Photoresponsive Ultrathin Graphitic-Phase C3N4 Nanosheets for Bioimaging. X. D. Zhang , X. Xie , H. Wang, J. J. Zhang, B. C. Pan and Y. Xie, *J. Am. Chem. Soc.,* 2013, **135,** 18-21.

[32] X. J. She, H. Xu, Y. G. Xu, J. Yan, J. X. Xia, L. Xu, Y. H. Song, Y. Jiang, Q. Zhang and H. M. Li, *J. Mater. Chem. A,* 2014, *2,* 2563-2570.

[33] P. Niu, L. L. Zhang, G. Liu and H. M. Cheng. *Adv. Funct. Mater.* 2012, **22,** 4763-4770.

[34] J. Xu, L. W. Zhang, R. Shi and Y. F. Zhu, *J. Mater. Chem. A,* 2013, **1,** 14766-14772.

[35] Y. J. Zhang, A. Thomas, M. Antonietti and X. C. Wang, *J. Am. Chem. Soc.* 2009, **131,** 50-51.

[36] M. Tahir, C. B. Cao, F. K. Butt, S. Butt, F. Idrees, Z. Ali, I. Aslam, M. Tanveer, A. Mahmoodc and N. Mahmoodc, *CrystEngComm,* 2014, **16,** 1825-1830.

[37] J. Gao, Y. Zhou, Z. S. Li, S. C. Yan, N. N. Wang and Z. G. Zou, *Nanoscale,* 2012, **4,** 3687-3692.

[38] L. C. Chen, D. J. Huang, S. Y. Ren, T. Q. Dong, Y. W. Chi and G. N. Chen, *Nanoscale,* 2013,

5, 225-230.

[39] Y. G. Xu, H. Xu, L. Wang, Jia. Yan, H. M. Li, Y. H. Song, L. Y. Huang and G. B. Cai, *Dalton Trans.,* 2013, **42,** 7604-7613.

[40] J. Cai, Y. M. He, X. X. Wang, L. H. Zhang, L. Z. Dong, H. J. Lin, L. H. Zhao, X. D. Yi, W. Z. Weng and H. L. Wan, *RSC Adv.,* 2013, **3,** 20862-20868.

[41] J. Y. Xu, Y. X. Li, S. Q. Peng, G. X. Lu, S. B. Li, *Phys. Chem. Chem. Phys,* 2013, **15,** 7657-7665.

[42] X. J. Bai, L. Wang, R. L. Zong and Y. F. Zhu. *J. Phys. Chem. C,* 2013, **117,** 9952-9961.

[43] D. M. Chen, K. W. Wang, D. G. Xiang, R. L. Zong, W. Q. Yao, Y. F. Zhu, *Appl. Catal. B.,* 2014*,* **147,** 554-561.

[44] H. L. Gao, S. C. Yan, J. J. Wang and Z. G. Zou, *Dalton Trans.,* 2014, **43,** 8178-8183.

[45] F. Bin, C. L. Song, G. Lv, J. O. Song, S. H. Wu, X. D. Li, *Appl. Catal. B.,* 2014, **150-151,** 532-543.

[46] Y. Wang, X. C. Wang and M. Antonietti, *Angew. Chem. Int. Ed.* 2012, **51,** 68-89.

[47] S. P. Wang, C. J. Li, T. Wang, P. Zhang, A. Li and J. L. Gong. *J. Mater. Chem. A,* 2014, **2,** 2885-2890.

[48] G. S. Li, B. Jiang, S. N. Xiao, Z. C. Lian, D. Q. Zhang, J. C. Yu and H. X. Li, *Environ. Sci.: Processes Impacts,* 2014, **16,** 1975-1980.

[49] Hongqi Sun, Guanliang Zhou, Yuxian Wang, Alexandra Suvorova, and Shaobin Wang, *ACS Appl. Mater. Interfaces,* 2014, **6,** 16745-16754.

[50] S. Shi, M. A. Gondal, A. A. A. Saadi, R. Fajgar, J. Kupcik, X. F. Chang, K. Shen, Q. Y. Xu, Z. S. Seddigi, *J. Colloid Interface Sci.,* 2014, **416,** 212-219.

[51] F. Chang, Y. C. Xie, J. Zhang, J. Chen, C. L. Li, J. Wang, J. R. Luo, B. Q. Denga, X. F. Hu *RSC Adv.*, 2014, **4,** 28519-28528.

Graphics captions

Fig. 1 The Z-potential of the samples.

Fig. 2 The SEM image of the g-C_3N_4 (A), g-C_3N_4-HNO_3 (B), g-C_3N_4-HNO_3-300 (C) and g-C_3N_4-HNO_3-500 (D), Fig. 2 (E) The proposed possible formation process of the nano-size g-C_3N_4.

Fig. 3 The XRD of the samples.

Fig. 4 The IR spectra of g-C_3N_4 (a), g-C_3N_4-HNO_3 (b), g-C_3N_4-HNO_3-300 (c) and g-C_3N_4-HNO_3-500 (d).

Fig. 5 The TG and DTA of the g-C_3N_4 (A) and g-C_3N_4-HNO_3 (B).

Fig. 6 The DRS spectra (A) and E_g (B) of the samples.

Fig.7 The PL spectra of the samples.

Fig. 8 XPS survey spectra (A) and high-resolution XPS spectra of C 1s (B) N 1s (C) and O 1s (D) for the samples and VB (E).

Fig. 9 The comparison of the photoactivity of the samples in decomposition of MO in different reaction system: (a) g-C_3N_4, (b) g-C_3N_4 and 0.5 mL MB, (c) 0.5 mL MB, (d) g-C_3N_4-HNO_3-500, (e) g-C_3N_4-HNO_3-300 and (f) g-C_3N_4-HNO_3-300 and 0.5 mL MB.

Fig. 10 Photodegradation of MO by g-C_3N_4-HNO_3-300/MB system.

Fig. 11 Stability investigation of g-C_3N_4-HNO_3-300/MB system for four cycles.

Fig. 12 ESR spectra of DMPO-O_2•$^-$ in methanol (A) and DMPO-•OH in water (B) before and after visible light irradiation with different g-C_3N_4-HNO_3-300 system conditions.

Fig. 13 The possible reaction mechanism.

Table 1 The obtained C/H/N analysis results of the samples.

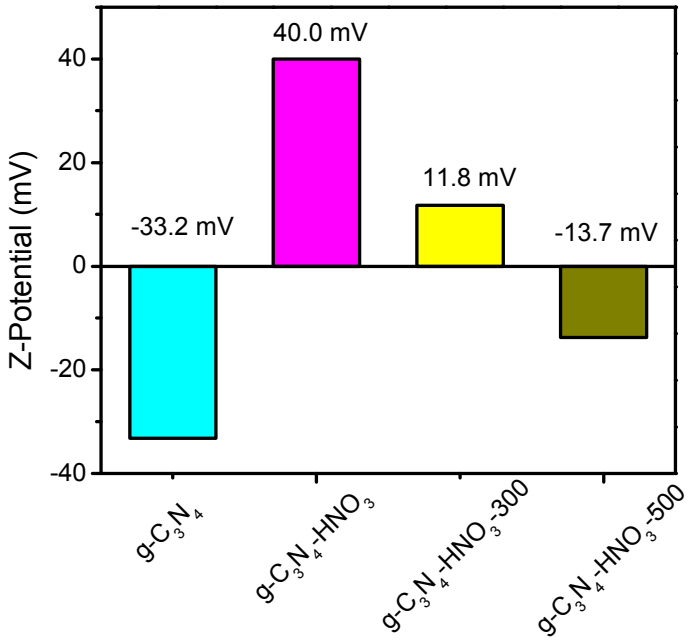

Fig. 1 The Z-potential of the samples.

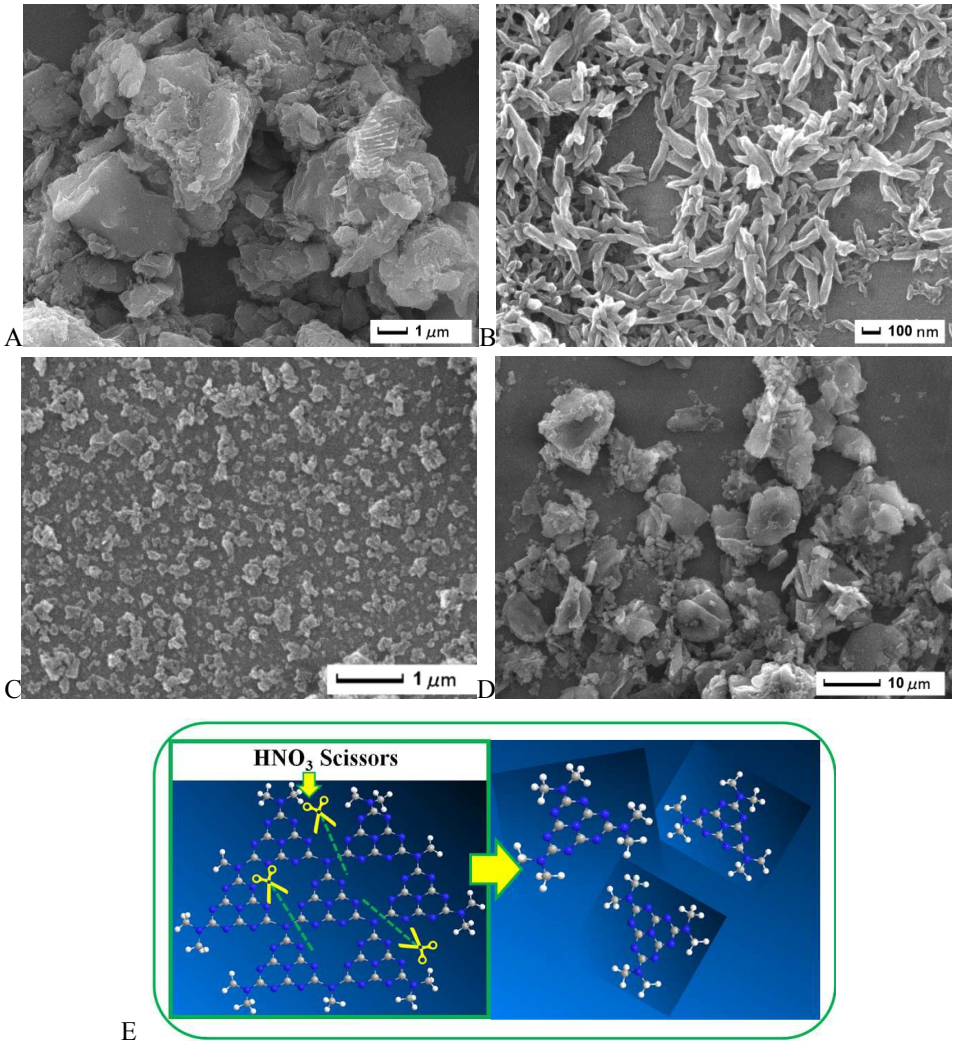

Fig. 2 The SEM image of the g-C_3N_4 (A), g-C_3N_4-HNO_3 (B), g-C_3N_4-HNO_3-300 (C) and g-C_3N_4-HNO_3-500 (D), Fig. 2 (E) The proposed possible formation process of the nano-size g-C_3N_4.

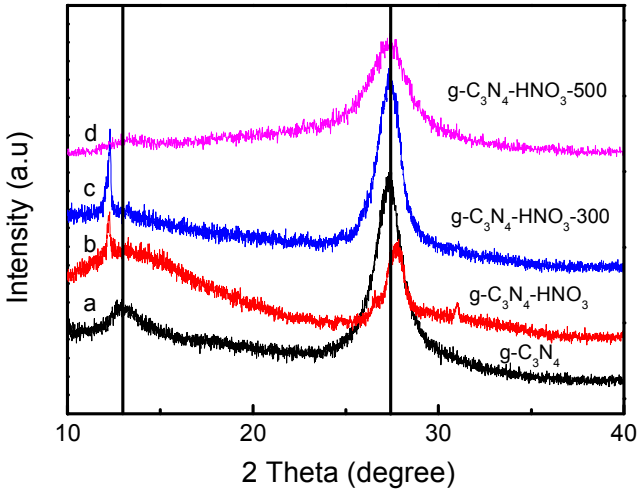

Fig. 3 The XRD of the samples.

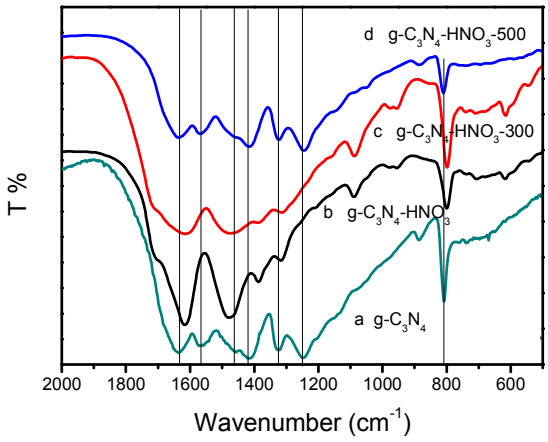

Fig. 4 The IR spectra of g-C_3N_4 (a), g-C_3N_4-HNO_3 (b), g-C_3N_4-HNO_3-300 (c) and g-C_3N_4-HNO_3-500 (d).

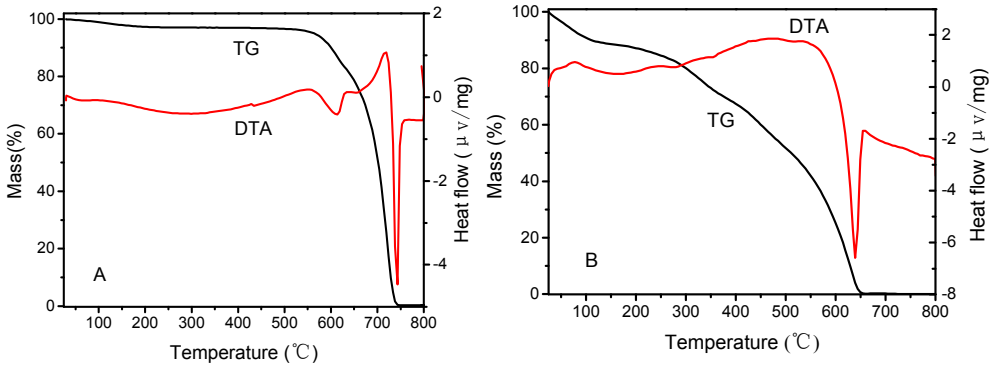

Fig. 5 The TG and DTA of the g-C_3N_4 (A) and g-C_3N_4-HNO_3 (B).

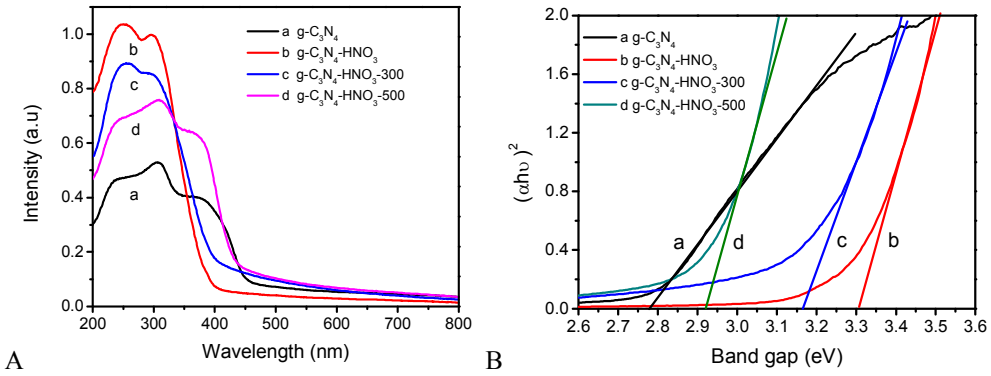

Fig. 6 The DRS spectra (A) and E_g (B) of the samples.

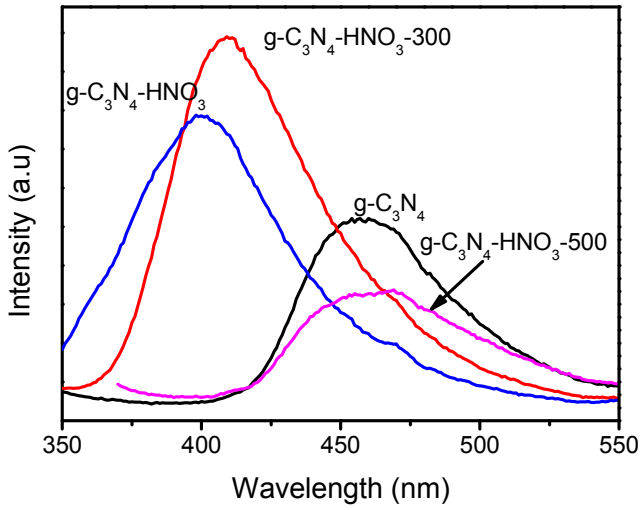

Fig.7 The PL spectra of the samples.

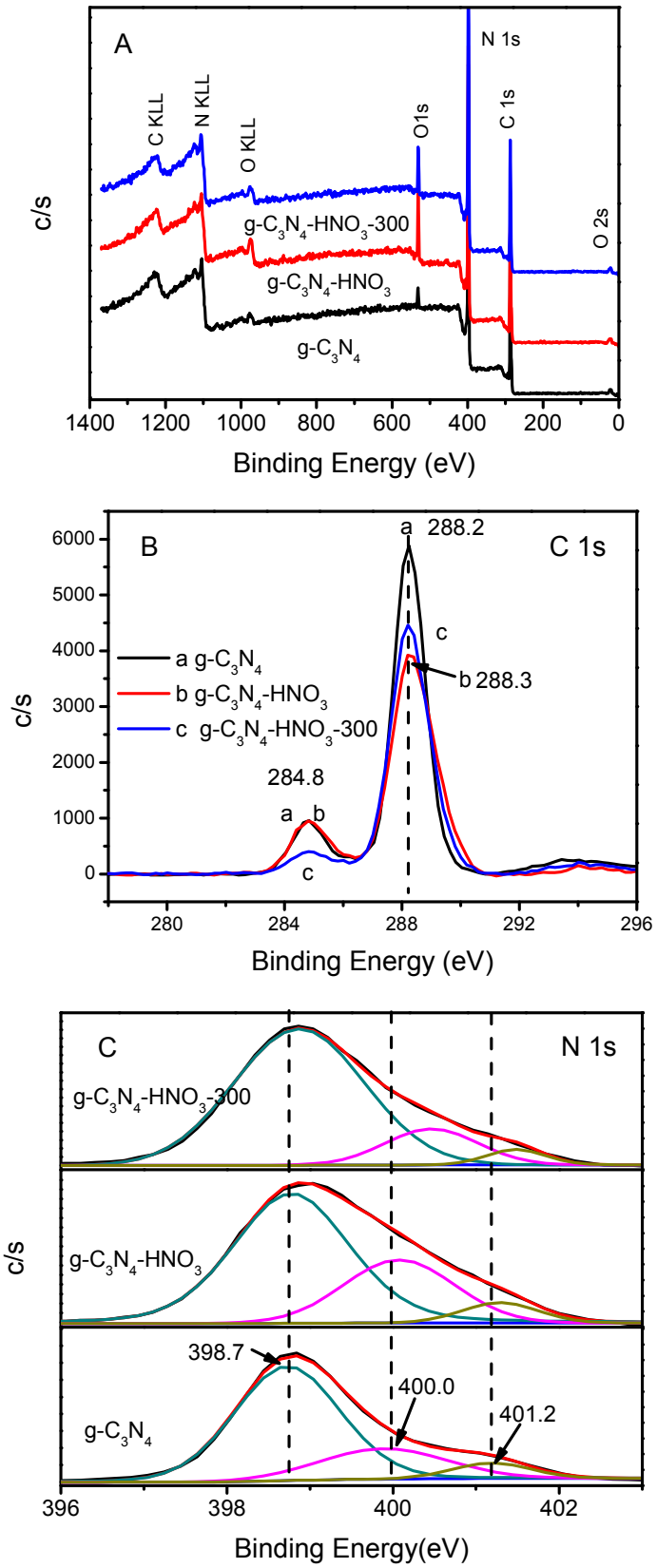

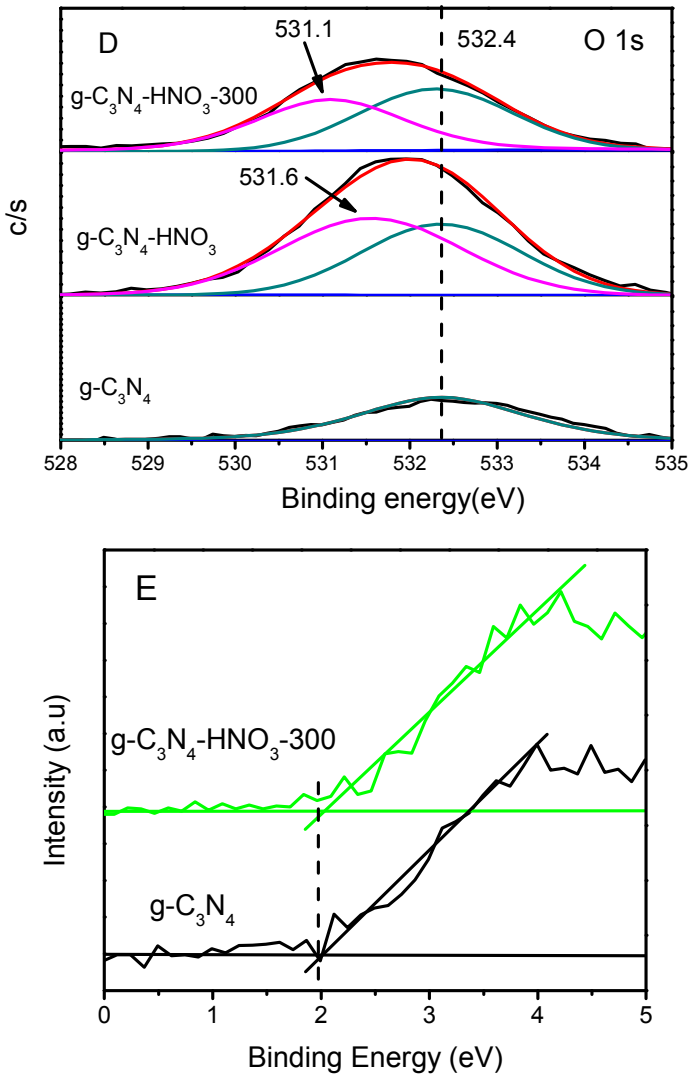

Fig. 8 XPS survey spectra (A) and high-resolution XPS spectra of C 1s (B) N 1s (C) and O 1s (D) for the samples, and VB (E).

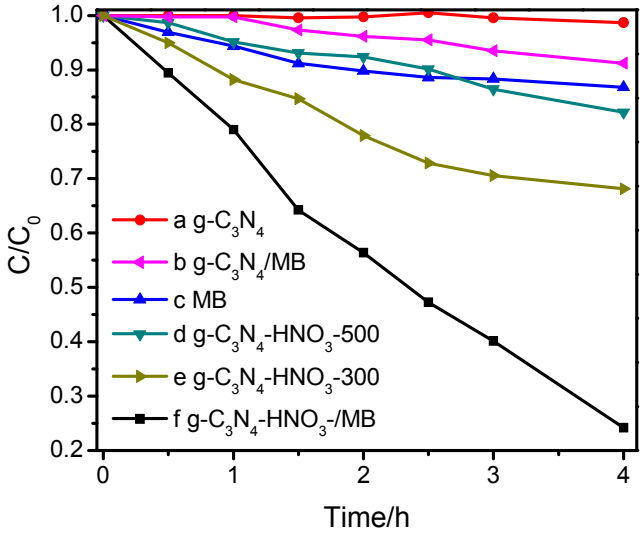

Fig. 9 The comparison of the photoactivity of the samples in decomposition of MO in different reaction system: (a) g-C_3N_4, (b) g-C_3N_4 and 0.5 mL MB, (c) 0.5 mL MB, (d) g-C_3N_4-HNO_3-500, (e) g-C_3N_4-HNO_3-300 and (f) g-C_3N_4-HNO_3-300 and 0.5 mL MB.

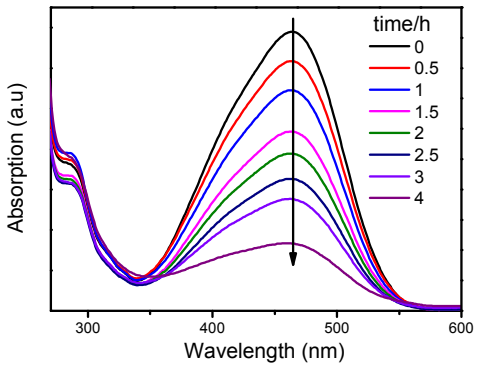

Fig. 10 Photodegradation of MO by g-C_3N_4-HNO_3-300/MB system.

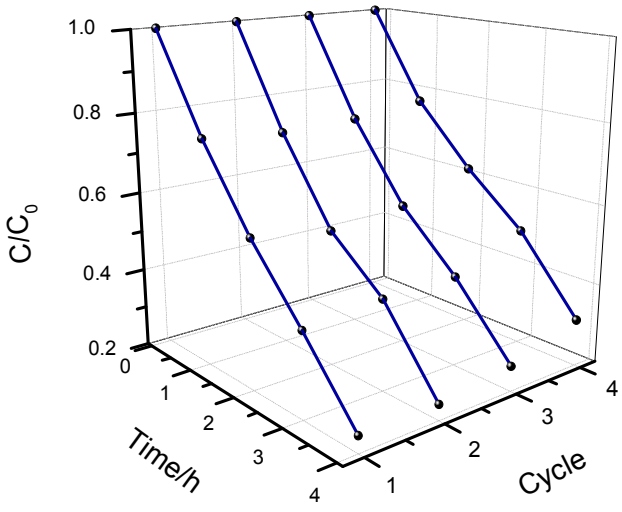

Fig. 11 Stability investigation of g-C_3N_4-HNO_3-300/MB system for four cycles.

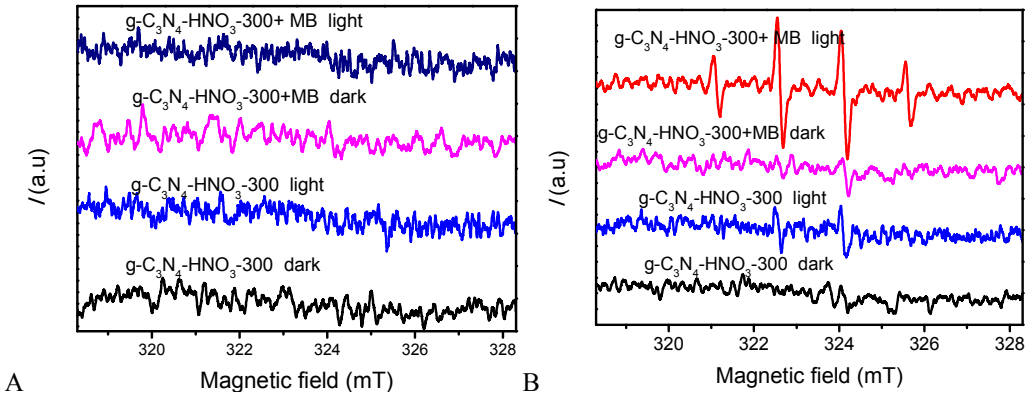

Fig. 12 ESR spectra of DMPO-O_2•$^-$ in methanol (A) and DMPO-•OH in water (B) before and after visible light irradiation with different g-C_3N_4-HNO_3-300 system conditions.

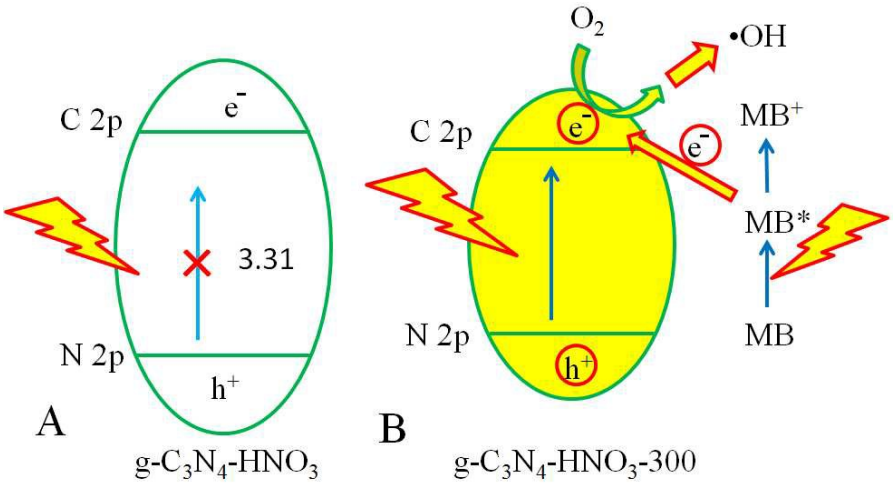

Fig. 13 The possible reaction mechanism.

Table 1 The obtained C/H/N analysis results of the samples.

	Elemental compositon				
	N (wt%)	C (wt%)	H (wt%)	O (wt%)	C/N (Atomic ratio)
g-C_3N_4	58.8	33.5	2.1	5.6	0.664
g-C_3N_4-HNO_3	51.3	26.3	3.7	18.7	0.598
g-C_3N_4-HNO_3-300	56.1	30.0	3.0	10.9	0.624
g-C_3N_4-HNO_3-500	57.0	32.3	2.3	8.4	0.660

Graphical Abstract

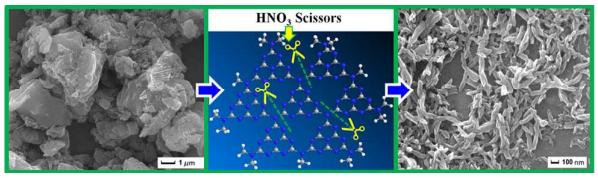

Bulk g-C_3N_4 was “cut” into nano-size g-C_3N_4 by HNO_3 scissors.